

How to identify a hyperbolic set as a blender

Stefanie Hittmeyer, Bernd Krauskopf, Hinke M. Osinga*

Department of Mathematics

The University of Auckland

Private Bag 92019

Auckland 1142, New Zealand

and Katsutoshi Shinohara

Graduate School of Business Administration

Hitotsubashi University

2-1 Naka, Kunitachi

Tokyo 186-8601, Japan

April 2020

Abstract

A blender is a hyperbolic set with a stable or unstable invariant manifold that behaves as a geometric object of a dimension larger than that of the respective manifold itself. Blenders have been constructed in diffeomorphisms with a phase space of dimension at least three. We consider here the question of how one can identify, characterize and also visualize the underlying hyperbolic set of a given diffeomorphism to verify whether it actually is a blender or not. More specifically, we employ advanced numerical techniques for the computation of global manifolds to identify the hyperbolic set and its stable and unstable manifolds in an explicit Hénon-like family of three-dimensional diffeomorphisms. This allows to determine and illustrate whether the hyperbolic set is a blender; in particular, we consider as a distinguishing feature the self-similar structure of the intersection set of the respective global invariant manifold with a plane. By checking and illustrating a denseness property, we are able to identify a parameter range over which the hyperbolic set is a blender, and we discuss and illustrate how the blender disappears.

1 Introduction

A blender is a hyperbolic set Λ (which we always assume to be transitive) of a diffeomorphism of dimension at least three whose characterizing property is that its stable manifold acts geometrically as a set of higher dimension. Blenders have been introduced by Bonatti and Díaz in 1996 [3] as examples of so-called robust non-uniformly hyperbolic systems, which represent a class of higher-dimensional chaotic dynamical systems with robustness properties.

The most famous example of a hyperbolic set is that of Smale's prototypical planar horseshoe map [24], which acts by the iterated stretching and folding of suitable rectangles; see also [22, 23] and textbooks on dynamical systems such as [10, 12, 20, 21]. All points that remain inside the initial rectangle for all time under both forward and backward iteration form its hyperbolic set Λ , which is a Cantor set in the plane that is topologically equivalent to the full shift on bi-infinite sequences of two symbols; one also speaks of a full horseshoe. Note that periodic points are dense in Λ and that it is transitive, that is, Λ has dense orbits. Moreover, Λ is a saddle set, meaning that it has a stable manifold $W^s(\Lambda)$ and an unstable manifold $W^u(\Lambda)$, which are defined as the points in phase space that converge to Λ in forward and backward time, respectively; these two global manifolds intersect transversely exactly in Λ . Horseshoe maps, or rather planar diffeomorphisms that are conjugate to a full shift on two symbols on an invariant set, arise in and are closely associated with homoclinic tangles of fixed or periodic points of planar diffeomorphisms; see, for example, [20, 21].

Bonatti and Díaz constructed a diffeomorphism in [3] for which they then gave a sufficient condition for the existence of the blender. A more intuitive way of constructing a blender is to think of it as the hyperbolic set of a generalization of Smale's horseshoe map to a higher-dimensional setting. This point of view is made very explicit in the recent introductory article of Bonatti, Crovisier, Díaz and Wilkinson [2], who present an affine model map in dimension three by adding a certain weak expansion and translation in a third variable. The result is the iterated stretching and folding of suitable rectangular boxes and, as these authors explain, the hyperbolic set Λ is a blender under suitable geometric conditions. In short, the question is when the hyperbolic set Λ generated by a three-dimensional horseshoe construction is a blender; see also [5].

There are a number of related definitions of the concept of blender [2, 3, 4, 5, 6, 7]; see also the discussion in [15, Sec. 2.1]. Throughout this work, we follow [7] and use [5, Definition 6.11]. For the case of a diffeomorphism with a three-dimensional phase space, it can be stated as follows [15]: a hyperbolic set Λ of unstable index 2 is called a *blender* if there exists a C^1 -open set of curve segments in the three-dimensional phase space that each intersect the one-dimensional stable manifold $W^s(\Lambda)$ locally near Λ . Moreover, this property must be robust, that is, hold for the corresponding hyperbolic set of every sufficiently C^1 -close diffeomorphism. Hence, colloquially speaking, $W^s(\Lambda)$ acts as if it were a surface; we also refer to this defining characteristic of a blender as the *carpet property*. It is very difficult to make a meaningful sketch, but imagine infinitely many parallel (infinitely thin) hairs or pieces of string that lie in accumulating disjoint layers, one in each layer. Such a set of hair has the carpet property if one 'cannot see through it' (when viewed from a directions transverse to the layers), even though its closure is not actually a surface. We believe that the best way to illustrate this property is by computing and visualizing Λ and $W^s(\Lambda)$, and we refer the reader already to Fig. 2(a): any curve segment in a C^1 -neighborhood of a straight line in the \bar{y} -direction locally near Λ (black dots) will intersect $W^s(\Lambda)$, represented by (finitely many) blue curve segments. Moreover, we also say that Λ is a blender when the unstable

index is 1 and the one-dimensional unstable manifold $W^u(\Lambda)$ has the carpet property. For an illustration of this case see already Fig. 4(a), where now any curve segment in a C^1 -neighborhood of a straight line in the \bar{x} -direction locally near Λ (black dots) will intersect $W^u(\Lambda)$ (represented by the red curves).

The constructions of blenders in the literature are abstract and not given in the form of a diffeomorphism with explicit equations. Hence, the question is how one can check in practice whether a hyperbolic set Λ is actually a blender, especially since specific diffeomorphisms arise in applications. The obvious first practical case, which we consider here, is that of a map defined on \mathbb{R}^3 . One approach, taken in [7] for the proof of the existence of a blender in a family of endomorphisms, is to identify a suitable three-dimensional box and verify required properties of how it returns under the given map. However, this is very technical and generally valid only in some neighborhood around a specified point in parameter space. Furthermore, the iterate needed for points to return to the box is typically very large, and this is hard to deal with from a practical point of view.

We present and extend here a complementary approach that was first suggested in [15]. The underlying idea is to employ advanced numerical methods to compute stable or unstable manifolds of suitable points in Λ in order to detect and illustrate its higher than expected dimensionality directly. In [15], one-dimensional stable or unstable manifolds of a fixed point $p \in \Lambda$ are computed to illustrate whether the hyperbolic set is a blender or not. Moreover, a numerical test for denseness in projection is presented, which is based on computing increasingly longer pieces of the respective one-dimensional global manifold; importantly, these are computed in a suitable compactification of the phase space \mathbb{R}^3 to handle excursion towards infinity. These methods were applied to a specific example of a family of diffeomorphisms with a blender.

Here, we use the same example that was introduced in [15], namely, the Hénon-like family

$$H(x, y, z) = (y, \mu + y^2 + \beta x, \xi z + y), \quad (1)$$

which is a perturbation of an endomorphism shown to have a blender in [7]. Importantly, the restriction to x and y of the family H , given by

$$h(x, y) = (y, \mu + y^2 + \beta x), \quad (2)$$

is conjugate to the Hénon map [14]. The z -coordinate of (1) is subject to a shear for which attraction or repulsion is given by the parameter and eigenvalue $\xi > 0$. The family H has the form of a skew-product system and H maps vertical lines (parallel to the z -axis) to vertical lines. Hence, the planar Hénon map h drives the z -dynamics but is itself not influenced by z . In other words, the properties of the (x, y) -dynamics are determined by the choice of the parameters μ and β , independently of the value for $\xi > 0$. This skew-product nature makes the map H a good test-case example that allows us to investigate important features of how blenders arise in a diffeomorphism given in explicit form beyond what has been reported in the literature.

We make use of known properties of the Hénon map and fix μ and β to ensure that the hyperbolic set Λ_h of h in the (x, y) -plane is that of a full horseshoe. Specifically, we fix throughout this work $\mu = -9.5$ and $\beta = 0.3$; note that $\beta = 0.1$ was considered in [15]. For this choice of parameters, the Hénon map h has two saddle fixed points

$$p_h^\pm := (\rho^\pm, \rho^\pm),$$

with

$$\rho^\pm := \frac{1}{2} \left((1 - \beta) \pm \sqrt{(1 - \beta)^2 - 4\mu} \right).$$

Their stable manifolds $W^s(p_h^\pm)$, which are defined as

$$W^s(p_h^\pm) := \{v \in \mathbb{R}^2 \mid h^k(v) \rightarrow p_h^\pm \text{ as } k \rightarrow \infty\},$$

and unstable manifolds $W^u(p_h^\pm)$, which are similarly defined as

$$W^u(p_h^\pm) := \{v \in \mathbb{R}^2 \mid h^{-k}(v) \rightarrow p_h^\pm \text{ as } k \rightarrow \infty\},$$

intersect transversely. The closure of $W^s(p_h^\pm) \cap W^u(p_h^\pm)$ is the hyperbolic set Λ_h , which is the maximal invariant set of h : it is a Cantor set on which h acts as the full shift on two symbols. Moreover, the stable manifold $W^s(\Lambda_h)$ of Λ_h is the closure of $W^s(p_h^\pm)$, and the unstable manifold $W^u(\Lambda_h)$ of Λ_h is the closure of $W^u(p_h^\pm)$.

These invariant sets are illustrated in Fig. 1, where we show the manifolds $W^s(p_h^\pm)$ (blue curves) and $W^u(p_h^\pm)$ (red curves) of the fixed points p_h^\pm (green crosses) as a good representation of the stable and unstable manifolds of Λ_h (black dots). Panel (a) shows a close-up of Λ_h in the (x, y) -plane, while panel (b) shows a larger part of the (x, y) -plane to illustrate the horseshoe-shapes of the stretching and folding global invariant manifolds. Finally, Fig. 1 (c) shows all invariant objects after compactification of the (x, y) -plane to the Poincaré disk (introduced formally in Eqs. (4) below), where the outer circle represents directions of approaches to infinity. Notice that $W^s(p_h^\pm)$ and $W^u(p_h^\pm)$ make long excursions towards a source s_h (red square) and a sink q_h (blue triangle), respectively, on the boundary of the Poincaré disk, which correspond to the vertical and horizontal asymptotes of approach to infinity that can be observed in panel (b). These images were generated by computing the stable and unstable manifolds as curves parameterized by arc-length with an adaptation of the algorithm described in [17] as implemented in the DSTOOL environment [1, 8, 19]; see already Section 2.

The properties of the planar map h imply certain properties of the family H in the three-dimensional phase space for the same choice $\mu = -9.5$ and $\beta = 0.3$. Indeed, H has two fixed points, given by

$$p^\pm := \left(\rho^\pm, \rho^\pm, \frac{\rho^\pm}{1 - \xi} \right). \quad (3)$$

They are also saddle points when ξ is positive and $\xi \neq 1$, because the corresponding fixed points p_h^\pm of h are saddles and the additional eigenvalue of p^\pm is ξ . Our central objects of study are the stable and unstable manifolds of the two fixed points p^\pm , which are defined as

$$\begin{aligned} W^s(p^\pm) &:= \{v \in \mathbb{R}^3 \mid H^k(v) \rightarrow p^\pm \text{ as } k \rightarrow \infty\} \quad \text{and} \\ W^u(p^\pm) &:= \{v \in \mathbb{R}^3 \mid H^{-k}(v) \rightarrow p^\pm \text{ as } k \rightarrow \infty\}. \end{aligned}$$

The dimensions of $W^s(p^\pm)$ and $W^u(p^\pm)$ depend on whether $0 < \xi$ is below or above one. Note that, due to the skew-product property of H , the vertical z -axis is an eigendirection of p^\pm . If $1 < \xi$ then $W^u(p^\pm)$ are two-dimensional manifolds and given by the direct product of $W^u(p_h^\pm)$ times \mathbb{R} ; more precisely, under backward iteration with H , the first two components of any point $v \in W^u(p_h^\pm)$ converge to the fixed point p_h^\pm of h , that is, the x - and y -components converge to ρ^\pm ,

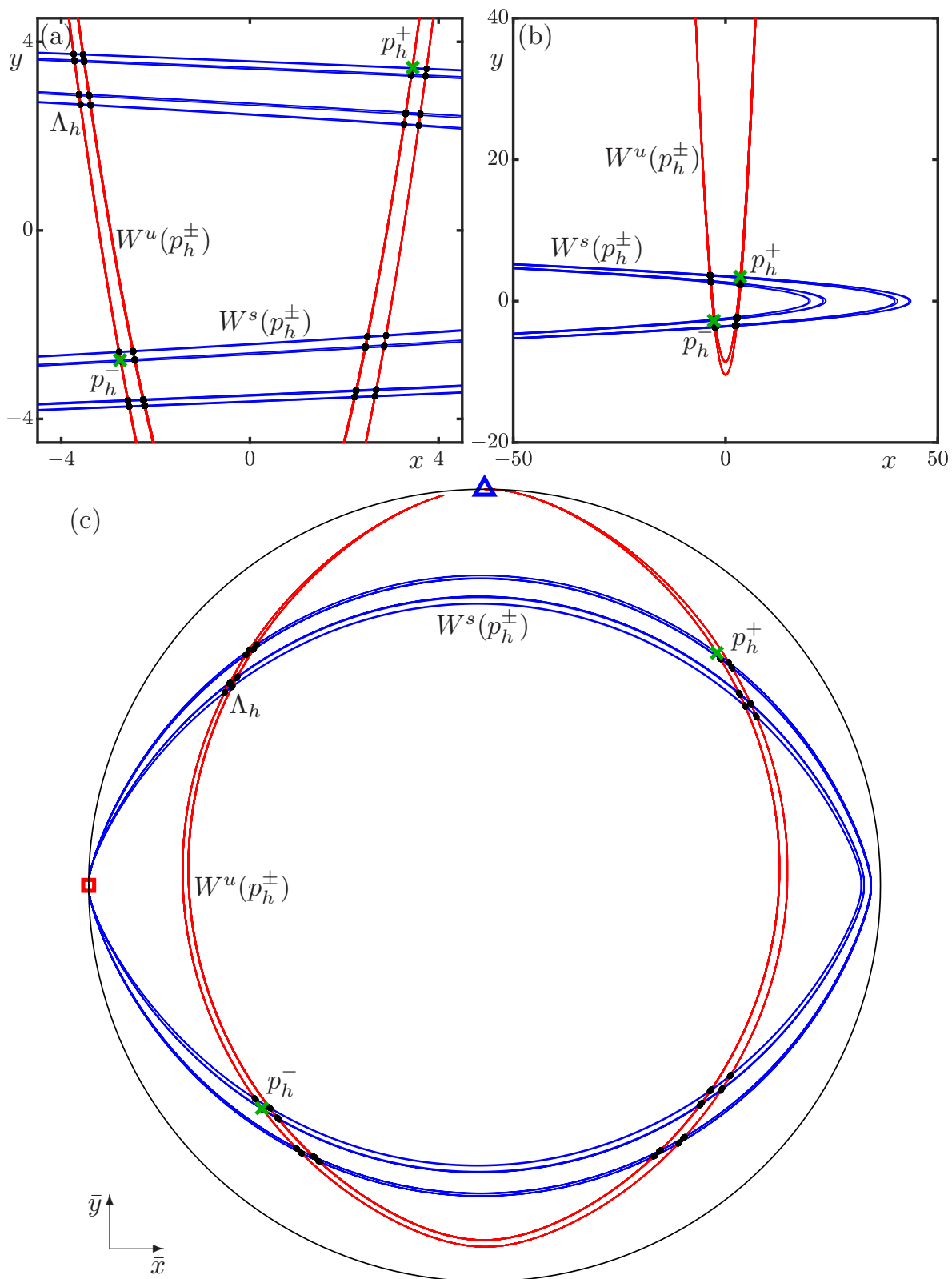


Figure 1: Illustration of the hyperbolic set Λ_h (black dots) as the closure of the intersection between the manifolds $W^s(p_h^\pm)$ (blue curves) and $W^u(p_h^\pm)$ (red curves) of the saddle fixed points p_h^\pm (green crosses); panels (a) and (b) show two views of the (x, y) -plane, and panel (c) shows the Poincaré disk in the (\bar{x}, \bar{y}) -plane.

and the z -component of v converges to $\rho^\pm/(1-\xi)$, which is the third component of p^\pm . Similarly, if $0 < \xi < 1$ then $W^s(p^\pm)$ are two dimensional and given by the direct product of $W^s(p_h^\pm)$ times \mathbb{R} . Hence, not only are the vertical projections of the saddles p^\pm onto the (x, y) -plane given by the fixed points p_h^\pm , but also the vertical projections of $W^s(p^\pm)$ and $W^u(p^\pm)$ onto the (x, y) -plane are the respective invariant manifolds $W^s(p_h^\pm)$ and $W^u(p_h^\pm)$ of the Hénon map h .

Consequently, H has a hyperbolic set Λ that is again the closure of the intersection set $W^s(p^\pm) \cap W^u(p^\pm)$; in particular, finding points in this intersection set is a good way of representing Λ . Moreover, its stable and unstable manifolds $W^s(\Lambda)$ and $W^u(\Lambda)$ are the closures of $W^s(p^\pm)$ and $W^u(p^\pm)$, respectively. As before, the vertical projections of the invariant sets Λ , $W^s(\Lambda)$ and $W^u(\Lambda)$ onto the (x, y) -plane are precisely the invariant sets Λ_h , $W^s(\Lambda_h)$ and $W^u(\Lambda_h)$ of the Hénon map h . We can check for the carpet property of Λ by considering the respective one-dimensional manifolds $W^s(p^\pm)$ when $1 < \xi$ and $W^u(p^\pm)$ when $0 < \xi < 1$. As we have seen in Fig. 1, these global manifolds have longer and longer excursion towards infinity before returning back to a neighborhood of Λ . While the algorithm we use to compute one-dimensional (un)stable manifolds can handle large excursions [17], such as those in Fig. 1(a) and (b), it is a much better approach to compactify the phase space \mathbb{R}^3 of (1) so that all excursions have a bounded arclength (rather than exponentially increasing ones). Indeed, we compute all global manifolds in compactified coordinates. This is not only more efficient and accurate, but also allows us to show the relevant global manifolds in their entirety, as in Fig. 1(c); see also [15].

In light of the skew-product nature of H , we consider the compactifying transformation

$$T(x, y, z) = (\bar{x}, \bar{y}, \bar{z}) := \left(\frac{x}{1 + \|(x, y)\|}, \frac{y}{1 + \|(x, y)\|}, \frac{z}{1 + |z|} \right), \quad (4)$$

to the interior of the cylinder

$$\mathcal{C} := \{(\bar{x}, \bar{y}, \bar{z}) \mid \|(\bar{x}, \bar{y})\| \leq 1 \text{ and } |\bar{z}| \leq 1\},$$

where $\|(\cdot, \cdot)\|$ is the Euclidean norm. Note that T is the product of the standard stereographic projection of the (x, y) -plane to the Poincaré disk and the stereographic compactification of the z -direction to the interval $[-1, 1]$. The conjugate map $T \circ H \circ T^{-1}$ is a map on (the interior of) \mathcal{C} ; for simplicity, we refer to this compactified map also as H , to its fixed points as p^\pm and to its hyperbolic set as Λ . The boundary $\partial\mathcal{C}$ of \mathcal{C} corresponds to directions of approaches to infinity in \mathbb{R}^3 , which by construction are represented as points on the boundary of the Poincaré disk in the first two coordinates and by a limiting slope in the z -direction. The map H can be extended to the boundary $\partial\mathcal{C}$ (see [15] for details), and this allows us to identify two sources $s^\pm := (-1, 0, \pm 1) \in \partial\mathcal{C}$ and two sinks $q^\pm := (0, 1, \pm 1) \in \partial\mathcal{C}$, which exist independently of $\xi > 0$. Note that q^\pm and s^\pm project to the source s_h and the sink q_h on the boundary of the Poincaré disk shown in Fig. 1(c).

In [15], we studied H for $\mu = -9.5$ and $\beta = 0.1$ and presented numerical evidence that the hyperbolic set Λ is a blender when $1 < \xi < \xi^* \approx 1.843$ and when $0.515 \approx \xi^{**} < \xi < 1$. To obtain this result we computed and showed for selected values of ξ the respective one-dimensional stable and unstable manifolds of only the fixed point p^- in the compactified phase space \mathcal{C} . They appear to have the carpet property of behaving as a surface when seen from an appropriate direction. This was checked by determining whether the largest gap in the respective projections of these curves converges to zero as a function of their arclength.

In this paper we consider the hyperbolic set Λ of H for $\mu = -9.5$ and $\beta = 0.3$ and characterize it more fully and in a number of new ways; specifically:

1. We compute the actual hyperbolic set Λ by finding a large number of intersection points of the stable and unstable manifolds $W^s(p^\pm)$ and $W^u(p^\pm)$ of both p^- and p^+ . Moreover, we determine the tangents to the one-dimensional manifolds $W^s(p^\pm)$ and $W^u(p^\pm)$, respectively, at the computed points of Λ . We also show Λ together with its tangents in the original phase space \mathbb{R}^3 of H .
2. We present in considerable detail the properties of the intersection sets of the two manifolds $W^s(p^-)$ and $W^s(p^+)$ with the vertical plane through the points p^- and p^+ . In particular, we consider the self-similar structure of this set, which represents the properties of the hyperbolic set. For any $\xi > 0$, this intersection set features the same Cantor set in the x - or y -direction, namely, that generated by the planar Hénon map h ; see Fig. 1. However, its self-similar structure is much more intriguing in the sheared z -direction, where for the case of a blender this projection covers intervals.
3. The figures and their different sub-panels that we present as part of this work have been designed carefully to illustrate the relevant properties of the invariant sets Λ , $W^s(\Lambda)$ and $W^u(\Lambda)$, in particular, the carpet property or its absence. In this way, we aim to address a lack of realistic three-dimensional visual representations of blenders and their geometry in an explicit dynamical system — concepts that are very difficult to convey in the form of sketches. While we recognize that some of our figures, especially those of three-dimensional objects, may be somewhat difficult to interpret at first sight, we believe that they are still the best way to convey the underlying geometric properties. Indeed, they have the added advantage of showing the invariant objects of a concrete family of maps in explicit form, thus, answering the question: what does a blender actually look like? In this way, our figures clarify and shed new light on the question whether Λ is a blender or not.
4. We illustrate in a new way when Λ is a blender by showing the projections of computed intersection points of $W^s(p^-)$ and $W^u(p^-)$ as a function of $\xi > 0$. This shows that the carpet property is lost because infinitely many and increasingly wider gaps appear in the relevant projection; subsequently, the respective one-dimensional invariant manifold is a Cantor set of curves when seen from any direction, so that there no longer exists a C^1 -open set of curve segments that must intersect this set.

2 Existence of a blender for $1 < \xi$

When $1 < \xi$, the z -direction is expanding and the hyperbolic set Λ of the map H has unstable index 2. Hence, the question is whether the stable manifold $W^s(\Lambda)$ has the carpet property. This can be studied by finding the one-dimensional global manifolds $W^s(p^\pm)$ of the two saddle points p^+ and p^- . Also of interest, especially for finding Λ , are the two-dimensional global manifolds $W^u(p^\pm)$, which in the compactified space \mathcal{C} are given by the one-dimensional manifolds $W^u(p_h^\pm)$ of the planar Hénon map h times the interval $(-1, 1)$. It turns out that the surfaces $W^u(p^-)$ and $W^u(p^+)$ are extremely close together, which is why we only consider and show $W^u(p^-)$ in what follows.

Hence, we need to compute $W^s(p^\pm)$ and $W^u(p_h^-)$. Each of these curves consists of two branches — on either side of p^\pm or p_h^- — that can be parameterized by arclength. Being global objects, such one-dimensional invariant manifolds need to be found numerically. Crucially, any manifold

computation for the family H is performed in the compactified phase space; in this way, we keep the computed arclength (distance in \mathcal{C}) manageable. For this task we employ the algorithm from [17], which is efficient and accurate with established error bounds. A one-dimensional manifold is grown point by point until a specified arclength L is reached, where the stepsize is adjusted according to the curvature. The computed part of the manifold is then given as an arclength-parameterized, piecewise-linear representation that satisfies user-specified accuracy parameters. We use the implementation of this algorithm in the DS_{TOOL} environment [1, 8, 19] to compute an initial, long piece of the respective one-dimensional manifold. We import the manifold data into MATLAB to produce images and for further data processing. Moreover, such a first piece of manifold can then be doubled successively in arclength with an adapted version of the growth algorithm; see also [15].

Figures 2 and 3, for $\xi = 1.2$ and $\xi = 2.0$, respectively, show what can be achieved with this computational approach when it comes to checking and illustrating the carpet property. Each of these two figures consists of four panels that show the geometric properties of the hyperbolic set Λ in different ways; taken together, these figures suggest that Λ is a blender for $\xi = 1.2$, and that this is not the case for $\xi = 2.0$. Panels (a) are images in the $(\bar{x}, \bar{y}, \bar{z})$ -space of the respective invariant sets the points p^\pm (green dots), their stable manifolds $W^s(p^\pm)$ (the curves in two shades of blue), which intersect the unstable manifold $W^u(p^-)$ (the surface shown in transparent red) in the hyperbolic set Λ (black dots); the cylinder \mathcal{C} forming the compactified phase space is indicated by the two unit circles at $z = \pm 1$; the two squares on $\partial\mathcal{C}$ are the sources $s^\pm := (-1, 0, \pm 1)$. Compare also with Fig. 1(c) for orientation; this figure corresponds to the ‘top view’ of panels (a) and further illustrates the locations the fixed points and their invariant manifolds. Panels (b) of Figs. 2 and 3 show the projections of p^\pm (green dots), of the hyperbolic set Λ (black dots) and of the curves $W^s(p^\pm)$ (light and darker blue) onto the (\bar{x}, \bar{z}) -plane; this corresponds to the view of panels (a) along the \bar{y} -direction. Panels (c) illustrate in non-compactified coordinates, that is, in (x, y, z) -space, the hyperbolic set Λ (black dots) and its tangent space $T^s(\Lambda)$; here, $T^s(\Lambda)$ is represented by line segments that are tangent to $W^s(p^\pm)$ at the computed points in $W^s(p^\pm) \cap W^u(p^-)$, which are colored in different shades of green to indicate the groups of points in Λ in the four respective quadrants. Panels (d) show the projections of Λ and $T^s(\Lambda)$ from panels (c) onto the (x, z) -plane.

Figure 2 illustrates that the hyperbolic set Λ (black dots in all panels) is a blender for $\xi = 1.2$. The view of $(\bar{x}, \bar{y}, \bar{z})$ -space in panel (a) shows how $W^s(p^-)$ and $W^s(p^+)$ weave back and forth while approaching repeatedly the two sources on $\partial\mathcal{C}$. In the process, they appear to fill out an area of the projection onto the (\bar{x}, \bar{z}) -plane in panel (b). This is an illustration of the carpet property, that is, the denseness of $W^s(p^\pm)$ in this projection. The computed points of the hyperbolic set Λ appear to align along vertical segments. The properties of Λ are further illustrated in Fig. 2(c) and (d) in the original, non-compactified coordinates of H . Here the line segments at the computed points are in the tangent space $T^s(\Lambda)$. This representation illustrates the defining blender property that the stable manifold $W^s(\Lambda)$ cannot be avoided locally near Λ by rays along the \bar{y} -direction, and that this property is robust with respect to small changes of this direction. The curves $W^s(p^-)$ and $W^s(p^+)$ have been computed here up to arclengths 1,200 and 1,056, respectively, and the curve $W^u(p_h^-)$ up to arclength 83. The intersection set of $W^s(p^\pm)$ with $W^u(p^-)$ for these arclengths consists of the shown 19,680 points that represent Λ ; for clarity of the images, the surface $W^u(p^-)$ is only shown up to arclength 10 of $W^u(p_h^-)$. Clearly, there are still gaps in the projections of $W^s(p^\pm)$ and of $T^s(\Lambda)$ in Fig. 2(b) and (d), respectively. As we will see in Sec. 4, these gaps will indeed close as the manifolds are computed to increasingly larger arclengths, which will provide

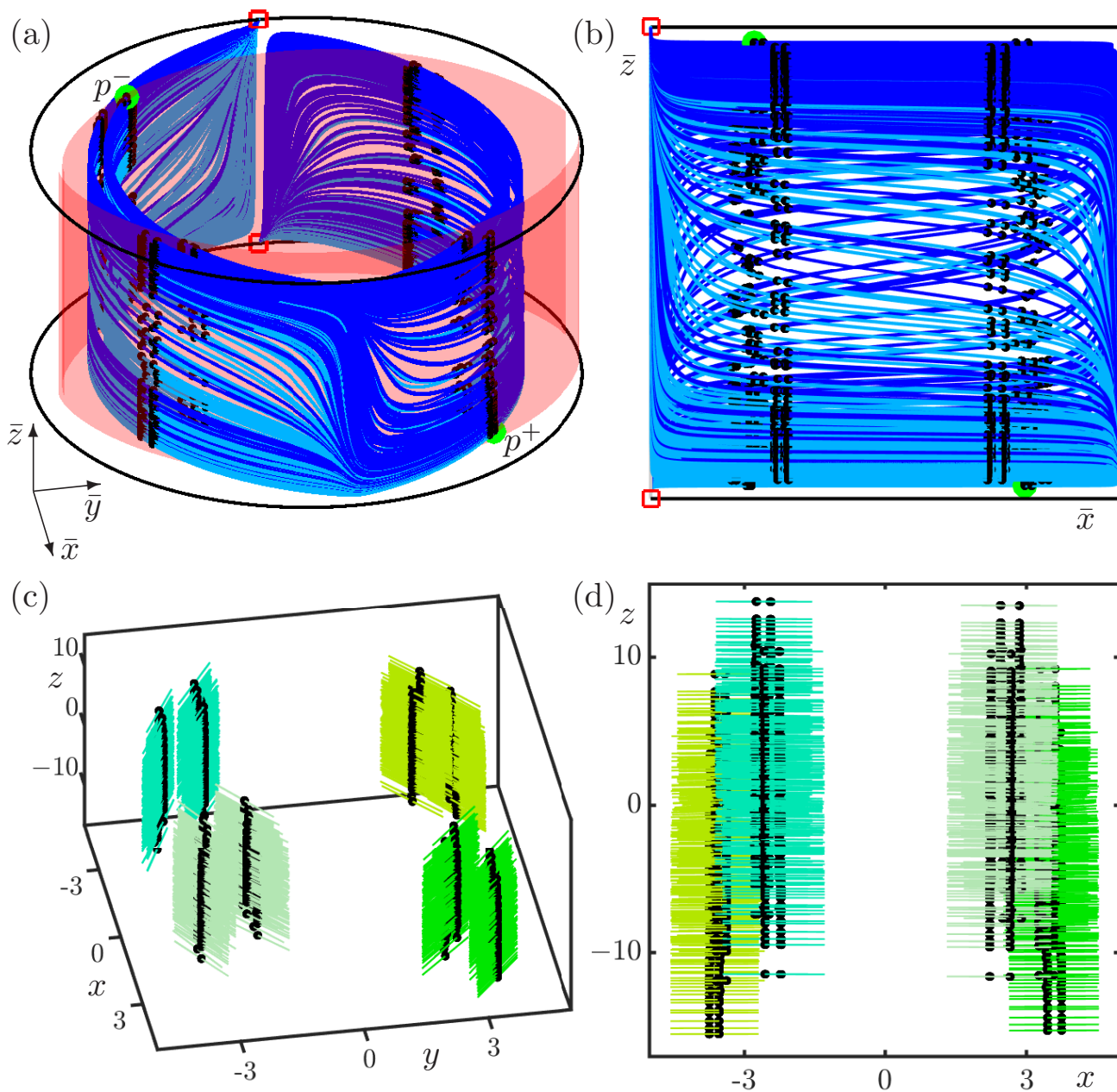


Figure 2: The hyperbolic set Λ (black dots) of H with $\xi = 1.2$, determined as the intersection set of $W^s(p^-)$ (dark blue) and $W^s(p^+)$ (light blue) with $W^u(p^-)$ (red surface), shown in $(\bar{x}, \bar{y}, \bar{z})$ -space (a) and in projection onto the (\bar{x}, \bar{z}) -plane (b). Panels (c) and (d) illustrate Λ and its tangent space $T^s(\Lambda)$ (green lines) in (x, y, z) -space and in projection onto the (x, z) -plane, respectively; four regions are highlighted with different shades of green.

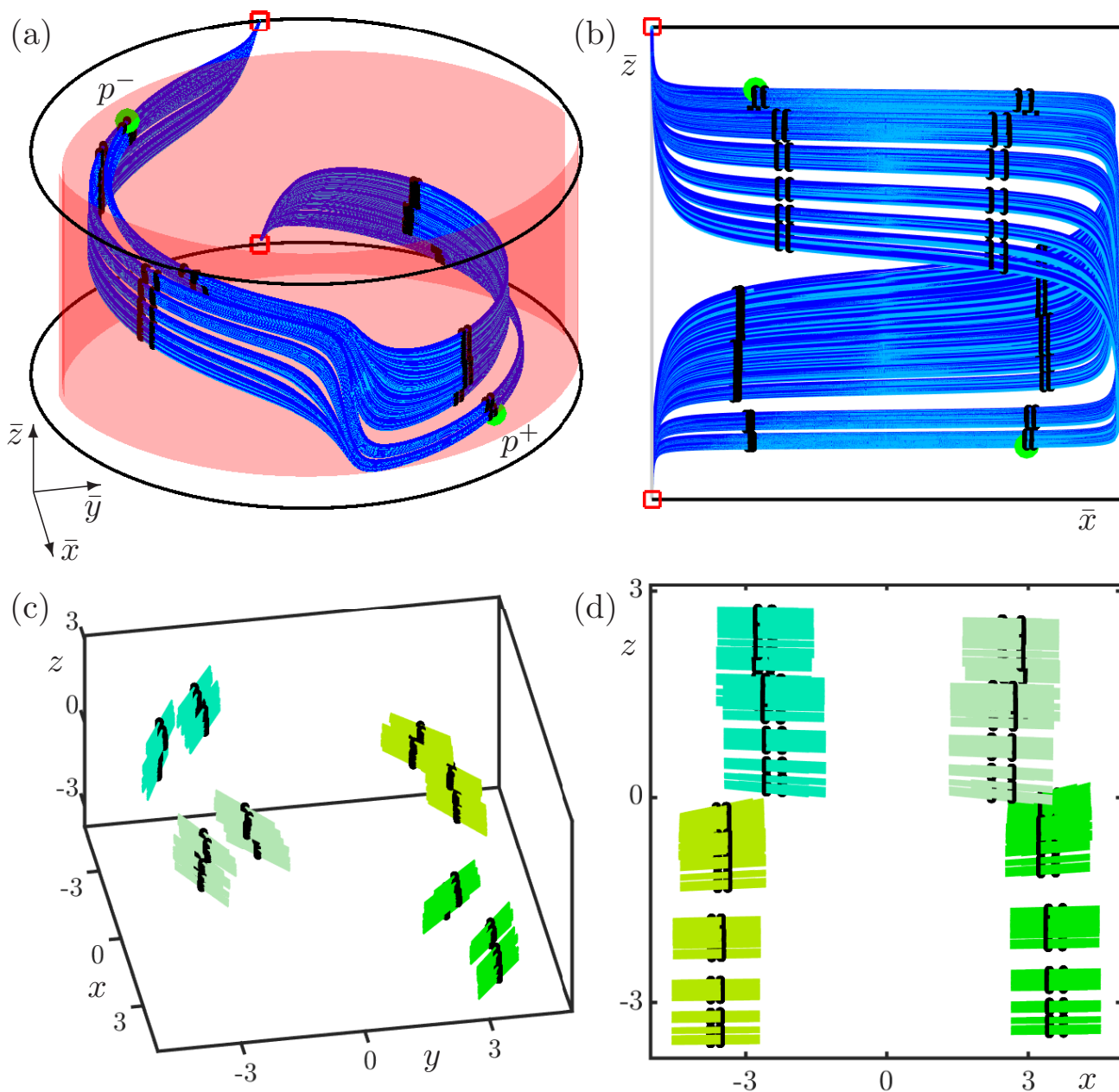


Figure 3: The hyperbolic set Λ (black dots) of H with $\xi = 2.0$, determined as the intersection set of $W^s(p^-)$ (dark blue) and $W^s(p^+)$ (light blue) with $W^u(p^-)$ (red surface), shown in $(\bar{x}, \bar{y}, \bar{z})$ -space (a) and in projection onto the (\bar{x}, \bar{z}) -plane (b). Panels (c) and (d) illustrate Λ and its tangent space $T^s(\Lambda)$ (green lines) in (x, y, z) -space and in projection onto the (x, z) -plane, respectively; four different regions are highlighted with different shades of green.

more comprehensive evidence that Λ is indeed a blender for $\xi = 1.2$.

When $\xi = 2.0$ as in Fig. 3, the properties of hyperbolic set Λ (black dots in all panels) are appreciatively different. The manifolds $W^s(p^\pm)$ are still weaving back and forth in panel (a) while approaching the two sources on $\partial\mathcal{C}$, but they no longer fill out a single large area of the (\bar{x}, \bar{z}) -plane in panel (b). Indeed, there are now consistent gaps in the \bar{z} -direction that do not fill up and, locally near Λ , appear to be a Cantor set of curve segments. This is confirmed by the images of Λ and $T^s(\Lambda)$ in panels (c) and (d). At the scale of Fig. 3(a) and (b), the manifolds $W^s(p^\pm)$ are a good representation of $W^s(\Lambda)$, meaning that computing these curves to larger arclengths would not change the image. Note that $W^s(p^-)$ and $W^s(p^+)$ have been computed up to very similar arclengths of 1,200 and 992, respectively. Again, the arclength of $W^u(p_h^-)$ is 83, there are 19,680 computed points of Λ , and the surface $W^u(p^-)$ is shown only up to arclength 10. The question of how the hyperbolic set Λ loses the carpet property when the expansion rate ξ is varied continuously from 1.2 to 2.0 will be addressed in Secs. 4 and 5.

3 Existence of a blender for $0 < \xi < 1$

When $0 < \xi < 1$, the z -direction is contracting, the hyperbolic set Λ has unstable index 1 and we now compute and check the one-dimensional global manifolds $W^u(p^\pm)$ for the carpet property. Their intersections with the surface $W^s(p^-)$, rendered from the curve $W^s(p_h^-)$, give the computed points in Λ . These objects, as well as $T^u(\Lambda)$, are shown in Figs. 4 and 5 for $\xi = 0.8$ and $\xi = 0.45$, respectively, suggesting that Λ is a blender for $\xi = 0.8$, while for $\xi = 0.45$ it is not. In the same style as before, panels (a) to (d) show representations of Λ and its manifolds or tangents in the $(\bar{x}, \bar{y}, \bar{z})$ -space, the (\bar{y}, \bar{z}) -plane, (x, y, z) -space and the (y, z) -plane, respectively. Note that panels (b) and (d) are now projections in the \bar{x} -direction and in the x -direction, respectively. Here $W^u(p^\pm)$ and $W^s(p_h^-)$ have been computed up to arclengths 800 and 57, respectively, to obtain 11,180 computed points of Λ ; for clarity of the illustrations, the surface $W^s(p^-)$ is only shown up to arclength 46 of $W^s(p_h^-)$. The curves $W^u(p^-)$ and $W^u(p^+)$ weave back and forth through Λ while now approaching repeatedly the two sinks $q^\pm := (0, 1, \pm 1)$ on the boundary $\partial\mathcal{C}$ of the cylinder \mathcal{C} (represented by the two circles in Figures 4 and 5). The question is whether $W^u(p^\pm)$ cover an area when projected in the \bar{x} -direction.

When $\xi = 0.8$ as in Fig. 4, the curves $W^u(p^-)$ and $W^u(p^+)$ lie very densely in panel (a) and appear to fill out a large area in the (\bar{y}, \bar{z}) -plane in panel (b). We conclude that the hyperbolic set Λ is a blender in this case. This is supported by the images in panels (c) and (d) of Λ with $T^u(\Lambda)$ in the non-compactified coordinates. As we checked, any gaps in the projection close as $W^u(p^\pm)$ are computed to larger arclengths; see Sec. 4. On the other hand, for $\xi = 0.45$ as in Fig. 5, there are clear gaps in projection along the x -direction that do not close when $W^u(p^\pm)$ are computed to larger arclength. Indeed, panels (a) and (b) suggest that the computed part of $W^u(p^\pm)$ is a good representation of the unstable manifold $W^u(\Lambda)$. The hyperbolic set Λ with $T^u(\Lambda)$ in panels (c) and (d) clearly shows a Cantor structure in the z -direction.

4 Verifying the carpet property

We now characterize in more detail the properties of the one-dimensional manifolds $W^s(p^-)$ and $W^s(p^+)$ when $1 < \xi$. To this end, we consider a plane Σ that is transverse to $W^s(p^\pm)$ and the

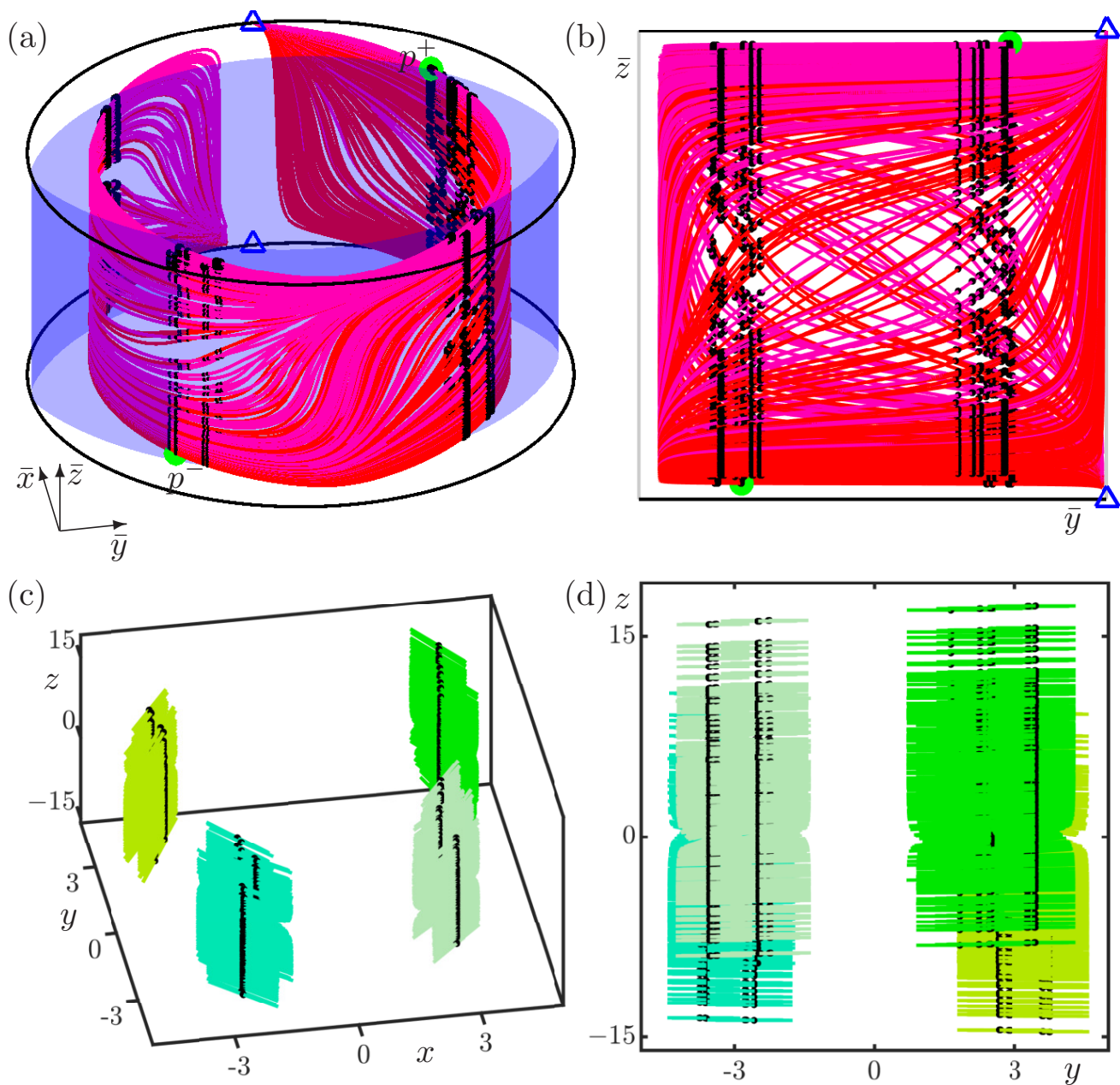


Figure 4: The hyperbolic set Λ of H with $\xi = 0.8$, determined as the intersection set of $W^u(p^-)$ (red curves) and $W^u(p^+)$ (magenta curves) with $W^s(p^-)$ (blue surface), shown in $(\bar{x}, \bar{y}, \bar{z})$ -space (a) and in projection onto the (\bar{y}, \bar{z}) -plane (b). Panels (c) and (d) illustrate Λ and its tangent space $T^s(\Lambda)$ (green lines) in (x, y, z) -space and in projection onto the (y, z) -plane, respectively; four regions are highlighted with different shades of green.

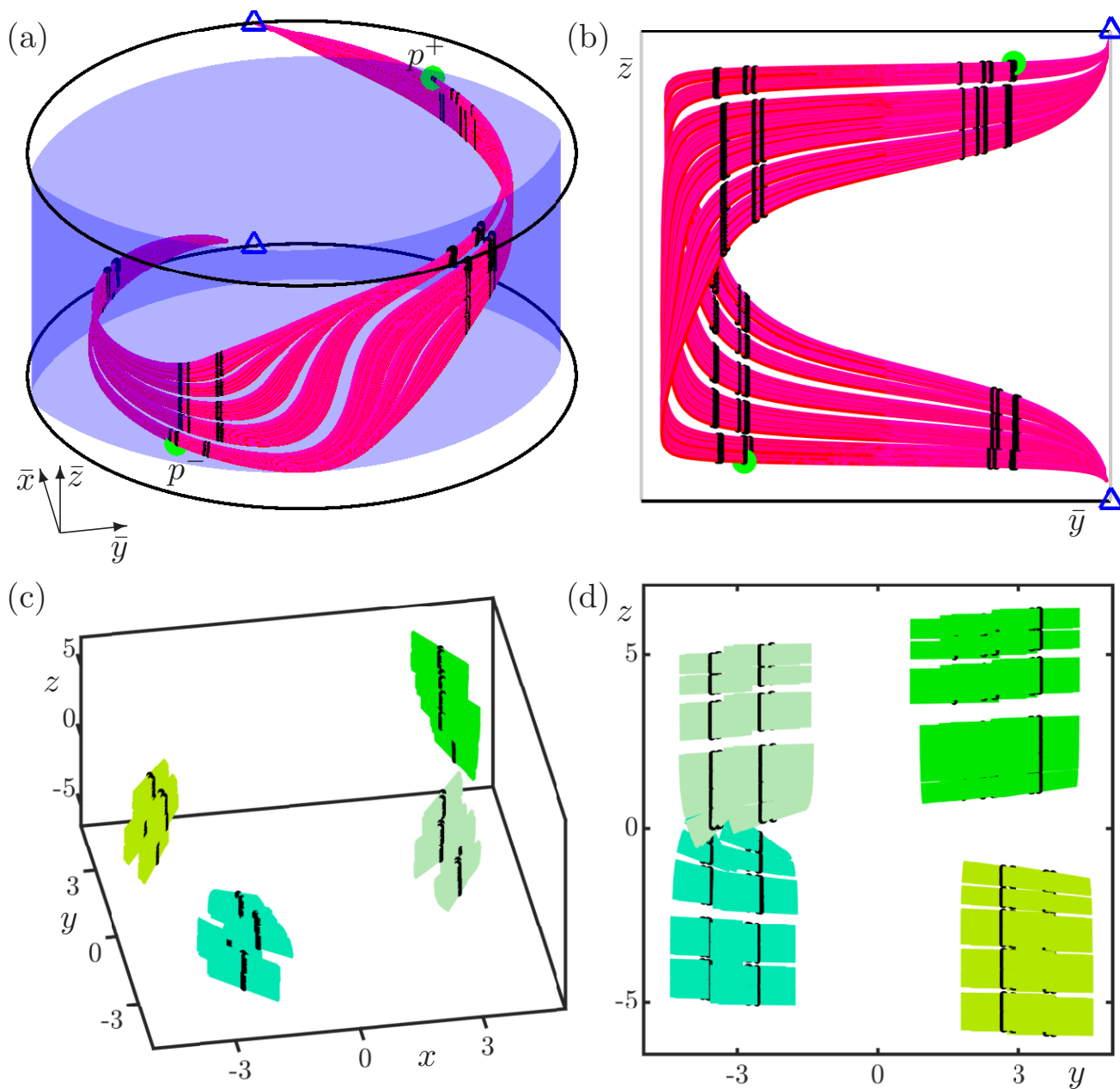


Figure 5: The hyperbolic set Λ of H with $\xi = 0.45$, determined as the intersection set of $W^u(p^-)$ (red curves) and $W^u(p^+)$ (magenta curves) with $W^s(p^-)$ (blue surface), shown in $(\bar{x}, \bar{y}, \bar{z})$ -space (a) and in projection onto the (\bar{y}, \bar{z}) -plane (b). Panels (c) and (d) illustrate Λ and its tangent space $T^s(\Lambda)$ (green lines) in (x, y, z) -space and in projection onto the (y, z) -plane, respectively; four regions are highlighted with different shades of green.

intersection set $W^s(p^\pm) \cap \Sigma$; a good choice for Σ is the vertical plane through the two fixed points p^- and p^+ , which in the compactified coordinates is given by

$$\Sigma := \{(\bar{x}, \bar{y}, \bar{z}) \in \mathcal{C} \mid \bar{x} = \bar{y}\}.$$

We illustrate in Figs. 6 and 7 the geometric intuition behind the computations that follow by showing how the curves $W^s(p^\pm)$ intersect the plane Σ containing the two fixed points p^- and p^+ , both for $\xi = 1.2$ when the hyperbolic set Λ appears to have the carpet property, and for $\xi = 2.0$ when it seemingly does not. Here the curves $W^s(p^\pm)$ have been computed to twice the arclength used in Figs. 2 and 3, respectively. Panels (a) of Figs. 6 and 7 show the situation in the plane Σ , where one finds the saddles p^\pm and the computed intersection points in $W^s(p^\pm) \cap \Sigma$. Panels (b), on the other hand, provide a three-dimensional image that serves to illustrate how the very long curves $W^s(p^\pm)$ inside the compactified cylinder \mathcal{C} weave back and forth through the plane Σ to create the intersection set $W^s(p^\pm) \cap \Sigma$.

Figure 6 for $\xi = 1.2$ is for the case that Λ is a blender. This can be deduced from the fact that the computed points in $W^s(p^\pm) \cap \Sigma$, when projected onto the vertical \bar{z} -axis in panel (a), appear to fill out the \bar{z} -interval bounded by p^- and p^+ . In other words, $W^s(p^\pm)$ has the carpet property with respect to directions near the horizontal in or near the plane Σ defined by $\bar{x} = \bar{y}$; this observation is confirmed by panel (b), which shows that this property is robust with respect to C^1 -small changes of the plane Σ . In contrast, the intersection set $W^s(p^\pm) \cap \Sigma$ for $\xi = 2.0$ in Fig. 7 is considerably smaller. Importantly, it no longer covers the \bar{z} -interval bounded by p^- and p^+ when projected onto the vertical \bar{z} -axis in panel (a); rather, there now appear to be some gaps (for example, above and quite close to p^+) through which a horizontal line can pass without intersecting $W^s(p^\pm)$. Again, panel (b) illustrates that this property is not specific to the chosen section Σ .

While Figs. 6 and 7 illustrate, or rather sketch, the geometric idea behind checking for the carpet property by looking for the emergence of gaps in a certain projection, they are by no means conclusive evidence by themselves. This is why we quantify this observation as follows. We order the \bar{z} -values of the computed N points of $W^s(p^-) \cap \Sigma$ to obtain the ordered set

$$\{\bar{z}_j\} \text{ with } \bar{z}_j \leq \bar{z}_{j+1}, \quad \text{where } j = 1, \dots, N.$$

We then compute the sequence of differences

$$\Delta^j = \bar{z}_{i+1} - \bar{z}_i, \quad \text{for } j = 1, \dots, N - 1,$$

and order the differences Δ^j in descending order to form the set $\{\Delta^i\}$, where $i = 1, \dots, N - 1$. Note that the number of points N and the \bar{z} -gaps Δ^i depend on the arclength L up to which $W^s(p^-)$ has been computed. In the compactified space \mathcal{C} , since the restriction h of H has a full horseshoe, we find effectively twice as many points in $W^s(p^-) \cap \Sigma$ every time this arclength is doubled. This allows us to consider the convergence properties of the Δ^i in dependence on the arclength as a numerical test to check for the carpet property.

Figure 8(a) shows the convergence of the first five successive maximal \bar{z} -gaps Δ^1 to Δ^5 . More specifically, we computed the Δ^i for the first pieces of $W^s(p^-)$ up to arclengths $L = 600 \cdot 2^k$, where k runs from 1 to 7; hence, the largest arclength of (each branch of) $W^s(p^-)$ for $k = 7$ used in this computation is 76,800 — which is an extremely long curve in the cylinder \mathcal{C} of diameter 2 and height 2. Note that we plot the logarithm of Δ^i against the exponent k , such that the

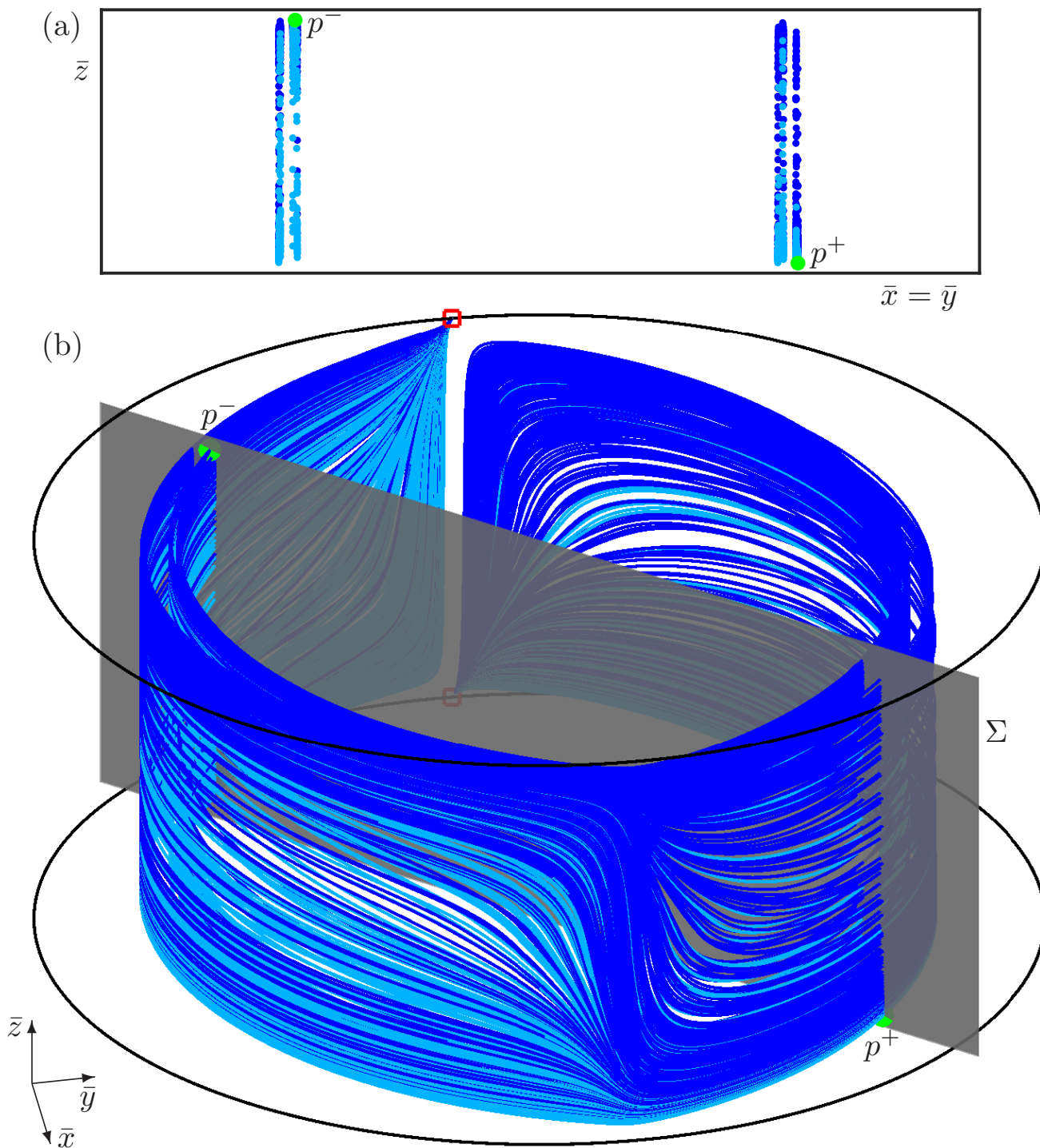


Figure 6: The intersection set for $\xi = 1.2$ of the stable manifolds $W^s(p^-)$ (dark blue) and $W^s(p^+)$ (light blue) with the section Σ (grey plane) defined by $\bar{x} = \bar{y}$. Panel (a) shows the intersection points in Σ and panel (b) shows how $W^s(p^\pm)$ intersect Σ in $(\bar{x}, \bar{y}, \bar{z})$ -space.

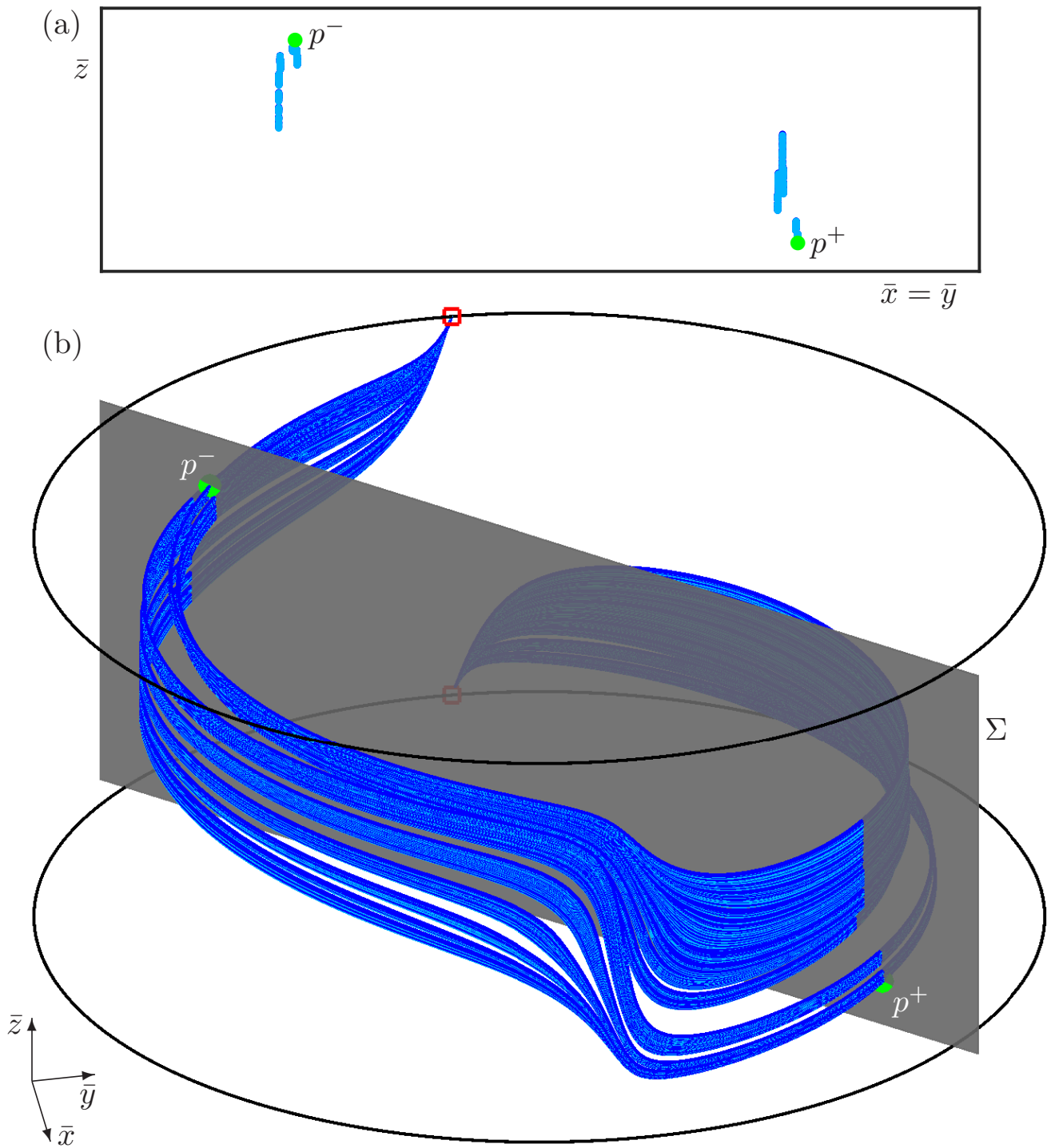


Figure 7: The intersection set for $\xi = 2.0$ of the stable manifold $W^s(p^-)$ (dark blue) and $W^s(p^+)$ (light blue) with the section Σ (grey plane) defined by $\bar{x} = \bar{y}$. Panel (a) shows the intersection points in Σ and panel (b) shows how $W^s(p^\pm)$ intersect Σ in $(\bar{x}, \bar{y}, \bar{z})$ -space.

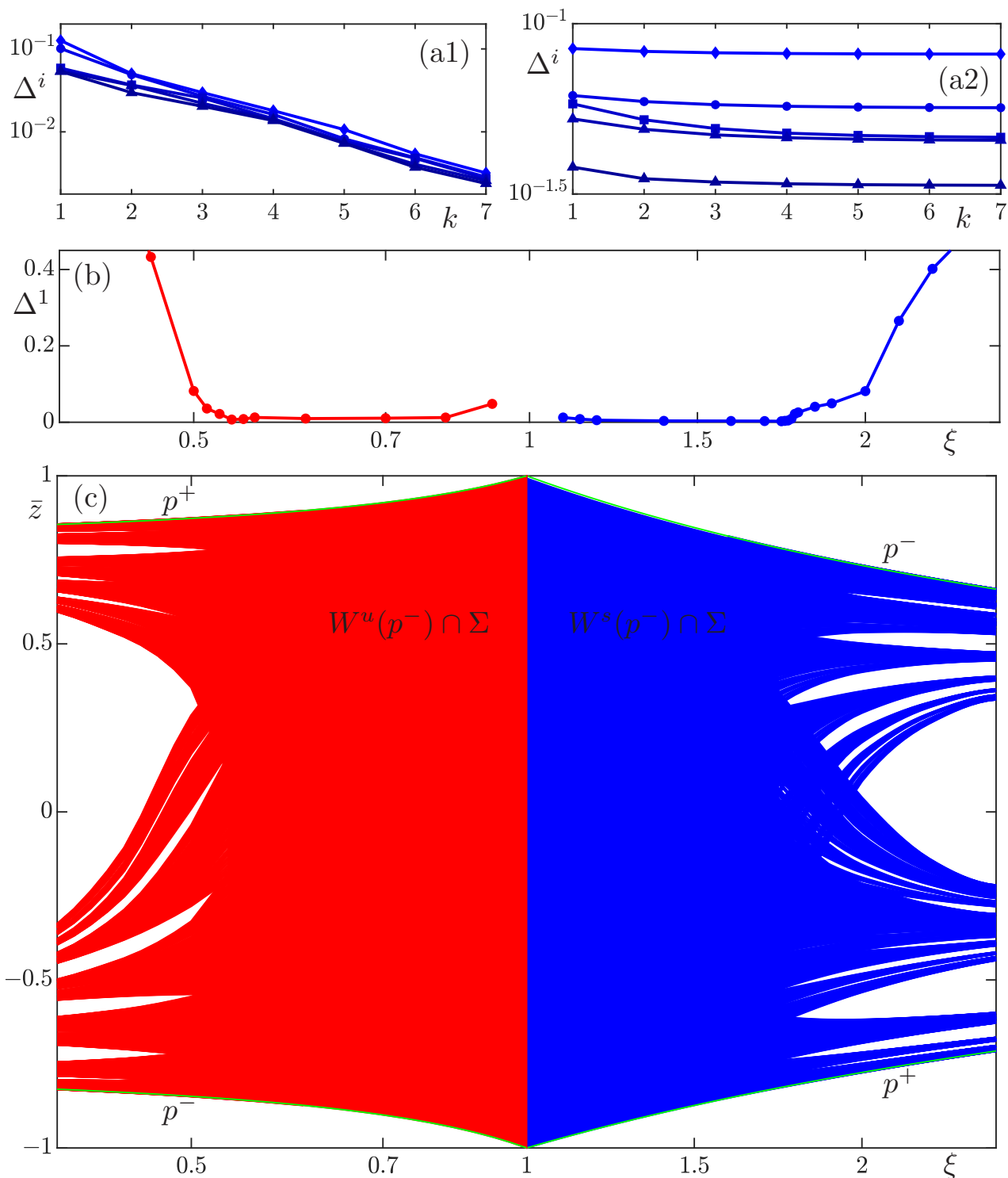


Figure 8: The five largest \bar{z} -gaps Δ^i , for $i = 1, \dots, 5$, of $W^s(p^-)$ in Σ as a function of the arclength, represented by the exponent k , for $\xi = 1.2$ (a1) and for $\xi = 2.0$ (a2). Panel (b) shows as a function of ξ the largest gap Δ^1 for $k = 7$ (red for $0 < \xi < 1$ and blue for $\xi > 1$) and panel (c) shows the associated \bar{z} -values of p^\pm (green) and of $W^s(p^-) \cap \Sigma$ (blue) and $W^u(p^-) \cap \Sigma$ (red), respectively.

rate of convergence to zero can be estimated as an approximately constant negative slope, while convergence to a fixed value is represented by a horizontal asymptote.

As Fig. 8(a1) shows, Δ^1 to Δ^5 clearly converge to zero for $\xi = 1.2$ as a function of k . This provides convincing evidence that Λ is indeed a blender in this case, as was already strongly suggested by Figs. 2 and 6. For $\xi = 2.0$, on the other hand, the \bar{z} -gaps Δ^1 to Δ^5 quickly reach nonzero limits, as is shown in Fig. 8(a2). Taken together, these two panels demonstrate that the criterion that the \bar{z} -gaps converge to 0 with k provides an convincing numerical test of the carpet property.

Figure 8(b) shows that this test allows us to determine over which ξ -range the carpet property is satisfied and Λ is a blender. Here we plot the maximal \bar{z} -gap Δ^1 as a function of ξ ; to achieve a better match with the half-line $1 < \xi$, we stretched the segment $0 < \xi < 1$ using the nonlinear transformation ξ to $2 - 1/\xi$, and the shown range starts with $\xi = 0.42$. The curve for $1 < \xi$ was determined by computing $W^s(p^-)$ for $k = 7$ at the ξ -values corresponding to the dots. Similarly, the curve for $0 < \xi < 1$ was determined from the intersection points of $W^u(p^-)$ with Σ ; here $W^u(p^-)$ was computed up to arclength $L = 200 \cdot 2^k$ with $k = 6$, that is, up to $L = 12,800$. While $\Delta^1 > 0$ for any such fixed-arclength computation, we observe a marked parabolic increase of Δ^1 for ξ sufficiently far away from 1. We determined the onset of this increase to two decimal places by computing Δ^1 for additional values of $\xi \in [0.50, 0.55]$ and $\xi \in [1.75, 1.80]$. We remark that it is a difficult task to determine precisely for which ξ the first gaps appear; see also [15] where we used a curve-fitting technique. Note that, due to the very weak contraction or expansion for ξ near 1, extremely large arclengths of the respective one-dimensional manifolds are required to cover $W^s(\Lambda)$ and $W^u(\Lambda)$ sufficiently; this is the reason why the points closest to $\xi = 1$ in Fig. 8(b), computed for the same fixed L , show Δ^1 as above zero. As we have checked, Δ^1 converges to zero also in this case, albeit very slowly; see also [15].

Our computations show that persistent gaps emerge approximately at $\xi = 0.53$ and $\xi = 1.75$. We conclude from our computations that the largest gap Δ^1 converges to zero as the arclength L of the respective manifold goes to infinity (as is illustrated in panel (a1) for $\xi = 1.2$) in the intervals $\xi \in [0.53, 1)$ and $\xi \in (1, 1.75]$. This, in turn, implies that the carpet property is satisfied and Λ is confirmed to be a blender in these ξ -ranges; see also [15]. To illustrate how the \bar{z} -gaps Δ^i arise outside the intervals $\xi \in [0.53, 1)$ and $\xi \in (1, 1.75]$, we show in Fig. 8(c) the projections onto the \bar{z} -interval of the sets $W^u(p^-) \cap \Sigma$ and $W^s(p^-) \cap \Sigma$ as a function of ξ . To obtain this image, the set of points $\{z_j\}$ in the respective intersection sets were computed for the maximal values of the arclengths above, and for the same ξ -values that were used to obtain panel (b). Here, the number N of intersection points z_j was taken constant in the calculations for $0 < \xi < 1$ and for $1 < \xi$, respectively. This allows us to connect by splines the corresponding points for different ξ of the ordered set $\{z_j\}$. In Fig. 8(c) the ξ -range where Λ is a blender clearly appears as a solid region bounded by the two fixed points p^- and p^+ . When the carpet property is lost, gaps emerge and continue to grow.

5 Further characterization of the carpet property for $1 < \xi$

In this section, we illustrate and characterize further what it means for the hyperbolic set Λ to have the carpet property or not. Here, we restrict our attention to the case $1 < \xi$ and consider the computed points in the intersection set $W^s(p^\pm) \cap \Sigma$ from Figs. 6 and 7 for $\xi = 1.2$ and for $\xi = 2.0$, respectively. Observe in Figs. 6(a) and 7(a) that the \bar{x} -coordinates (and thus, also the

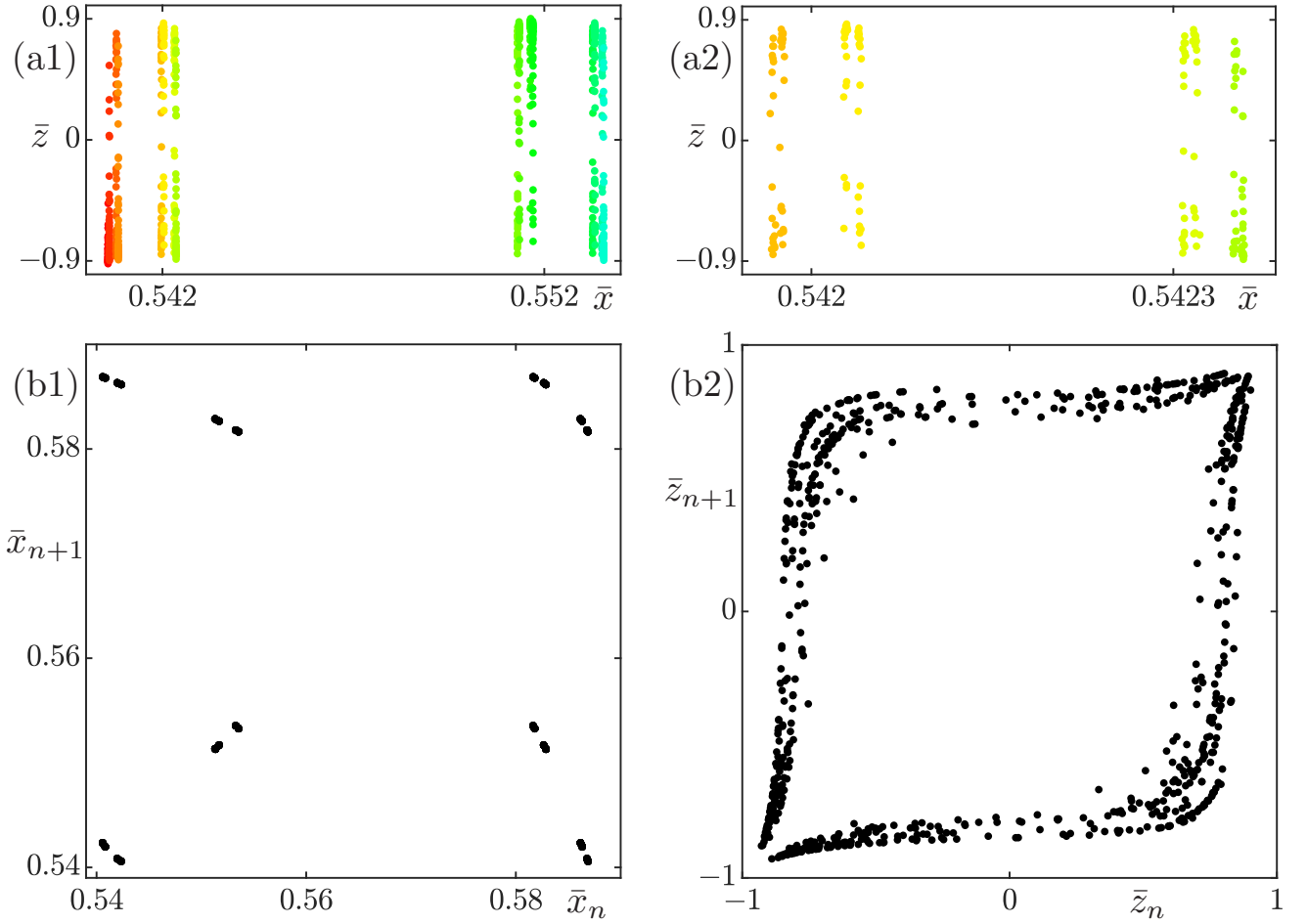


Figure 9: Self-similar structure of the intersection set $W^s(p^-) \cap \Sigma$ for $\xi = 1.2$. Panel (a1) shows a part of $W^s(p^-) \cap \Sigma$ in a color coding according to the \bar{x} -values, and panel (a2) is an enlargement. Panels (b1) and (b2) show \bar{x}_{n+1} versus \bar{x}_n and \bar{z}_{n+1} versus \bar{z}_n , respectively, of successive points of $W^s(p^-) \cap \Sigma$.

\bar{y} -coordinates) of the points in $W^s(p^\pm) \cap \Sigma$ appear to be organized in a self-similar structure. This is indeed the case, because of the Cantor structure of the underlying hyperbolic set Λ_h and its stable manifold $W^s(\Lambda_h)$, which is the closure of $W^s(p_h^-)$. One can discern four groups of points, two groups each for positive and negative \bar{x} -values, separated by small gaps just before the \bar{x} -coordinates of p^- and p^+ . We focus on the \bar{x} -range that corresponds to the third group of intersection points, that is, we consider the range $\bar{x} \in [0.540, 0.554]$ on the positive axis to the left of p^+ .

Figures 9 and 10 show this data in a new way that emphasizes the self-similar structure of $W^s(p^-) \cap \Sigma$. Here, panels (a1) reproduce the third group of points from Figs. 6(a) and 7(a), colored according to 32 different \bar{x} -ranges that correspond to intervals in the construction of the Cantor set along the \bar{x} -axis; in other words, all points of the same color represent a different group at this specific depth of the Cantor set construction. Note that these images again show four groups of points that seem similar to a mirrored version of Figs. 6(a) and 7(a). The subsequent panels (a2) each show an enlargement of the second group of points (compare the colors and the scale along the \bar{x} -axis); these panels also show four groups of points that seem similar to a mirrored version

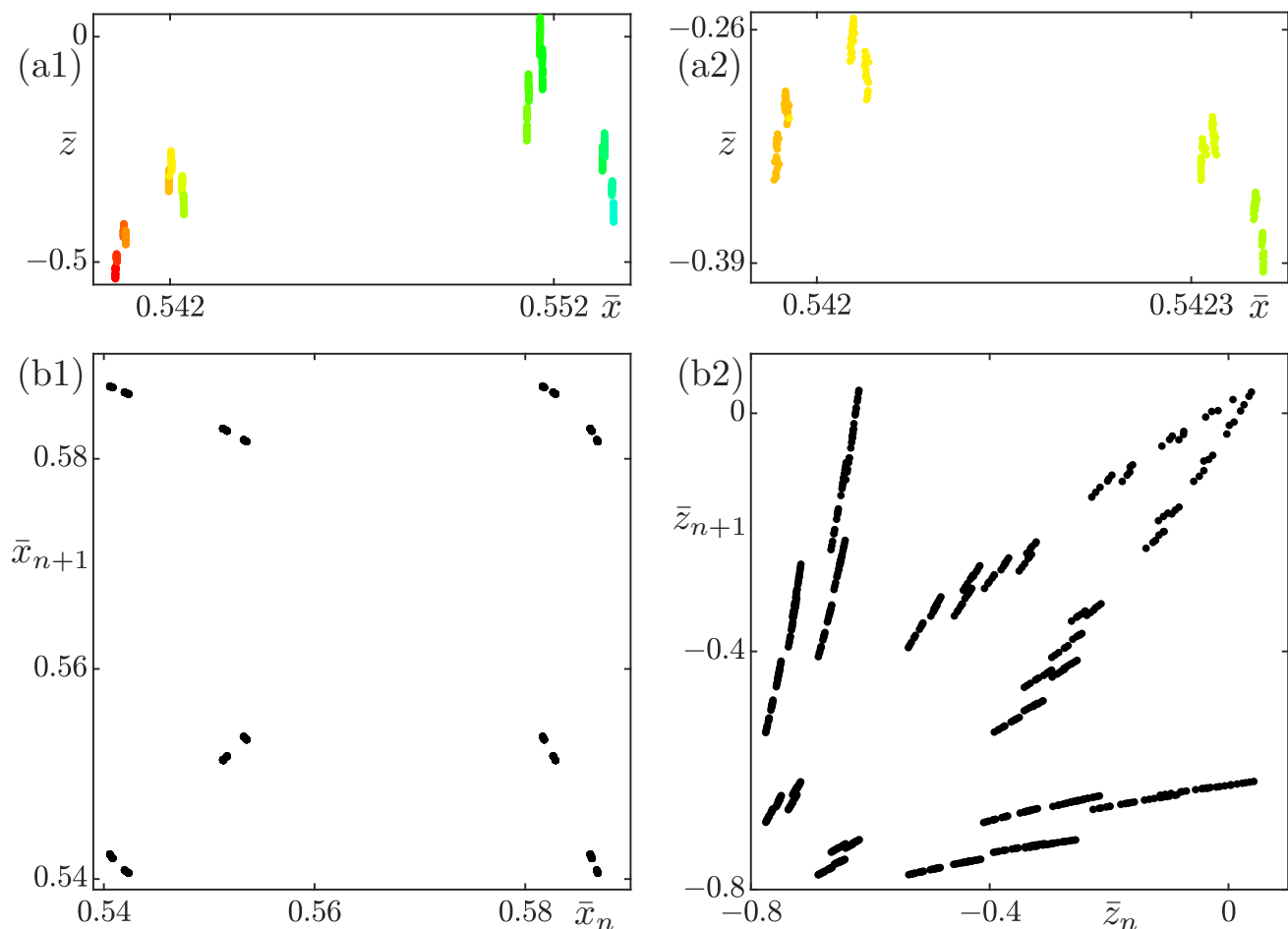


Figure 10: Self-similar structure of the intersection set $W^s(p^-) \cap \Sigma$ for $\xi = 2.0$. Panel (a1) shows a part of $W^s(p^-) \cap \Sigma$ in a color coding according to the \bar{x} -values, and panel (a2) is an enlargement. Panels (b1) and (b2) show \bar{x}_{n+1} versus \bar{x}_n and \bar{z}_{n+1} versus \bar{z}_n , respectively, of successive points of $W^s(p^-) \cap \Sigma$.

of those in panels (a1).

Panels (b1) and (b2) of Figs. 9 and 10 illustrate the self-similarity of this Cantor set in a different way. Here, we order the points in $W^s(p^-) \cap \Sigma$ as a first part of the bi-infinite sequence of successive intersection points $w_n = (\bar{x}_n, \bar{y}_n, \bar{z}_n) \in W^s(p^-) \cap \Sigma$, with $n \in \mathbb{Z}$, along both branches of $W^s(p^-)$; here, $w_0 = p^-$ and one branch of $W^s(p^-)$ corresponds to positive and the other to negative n . (The sequence of the arclength ordered points \bar{z}_n should not be confused with the ordered set $\{\bar{z}_j\}$ used in Sec. 4 to define the \bar{z} -gaps.) The sequence (w_n) is a finite part of the bi-infinite sequence of consecutive points in $W^s(p^-) \cap \Sigma$, and we are interested in the relation between w_n and w_{n+1} . Panels (b1) of Figs. 9 and 10 show the coordinates \bar{x}_{n+1} versus \bar{x}_n and panels (b2) show \bar{z}_{n+1} versus \bar{z}_n .

Figure 9 illustrates in a rather different way that the hyperbolic set Λ for $\xi = 1.2$ is a blender. Panels (a1) and (a2) illustrate the geometric principle of mapping a stretched and folded box back into itself [2]. Panel (a1) can be obtained from panel (a2), qualitatively and even quantitatively by taking into account that the enlargement has fewer points and a smaller set of colors, from a scaling combined with reflection in a vertical line through the center of panel (a2); a similar

scaling with reflection is needed when scaling panel (a1) back to Fig. 6(a). Scaling with reflection must also be applied to the the fourth group of points in panel (a1), while the self-similarity with the first and third groups does not require a reflection. Note that the associated contraction rates in the \bar{x} -direction and the \bar{z} -direction are very different. The contraction in the \bar{x} -direction is strong and the corresponding \bar{x} -intervals (indicated by different color) generate the Cantor set of the planar Hénon map. In the \bar{z} -direction, on the other hand, the contraction is much weaker, meaning that the corresponding \bar{z} -intervals of the same color overlap to a considerable extent; this overlap is a necessary ingredient for the generation of a blender in [2]. Figure 9(b1) and (b2) illustrate these contractions differently. The plot of \bar{x}_{n+1} versus \bar{x}_n in panel (b1) shows an immediate clustering in a Cantor set based on four groups along the \bar{x}_n - and \bar{x}_{n+1} -axes. The plot of \bar{z}_{n+1} versus \bar{z}_n in panel (b2), on the other hand, covers an entire \bar{z} -interval, which is another illustration of the carpet property.

Figure 10 represents the intersection set $W^s(p^-) \cap \Sigma$ for $\xi = 2.0$ in the same way and for the same groups of points with the same colors; namely, panel (a1) shows the left half of the points with positive \bar{x} in Fig. 7(a1) and panel (a2) is an enlargement of the second quarter of these points. The enlargement in panel (a2) is also very similar to panel (a1) when reflected in a suitable vertical. However, while the qualitative features agree well, obtaining self-similarity appears to involve a nonlinear transformation of the \bar{z} -direction. A notable difference with the case of $\xi = 1.2$ is that the corresponding \bar{z} -intervals of points of equal color in panel (a1) and (a2) no longer all overlap. As a result, there are now gaps in the horizontal projections of the points in $W^s(p^-) \cap \Sigma$ onto the \bar{z} -axis. This is due to the stronger contraction in the \bar{z} -direction. Note that the Cantor set along the \bar{x} -axis is always the same for any $1 < \xi$, which is why the plot of \bar{x}_{n+1} versus \bar{x}_n in Fig. 10(b1) remains unchanged. The plot of \bar{z}_{n+1} versus \bar{z}_n in panel (b2), on the other hand, is now very different from that in Fig. 9(b2).

An interesting observation in Fig. 10 is that there exist gaps in the vertical \bar{z} -direction in between certain colored sets of points (corresponding to a given level of the Cantor set box construction), while other colored sets of points still have a \bar{z} -overlap. This suggests that the stronger contraction rate in the \bar{z} -direction is not uniform and so certain \bar{z} -intervals of the blender box construction still overlap. In other words, as a function of the contraction rate ξ , gaps open up successively in different places. The conclusion is that the way a suitable box is mapped over itself is more complicated than the two-to-one map suggested in the abstract example from [2], which is the geometrically most straightforward generalization of the planar horseshoe construction to \mathbb{R}^3 . How exactly the structure of $W^s(\Lambda)$ changes with ξ , and what this means in terms of a sequence of contracting boxes, is the subject of ongoing research.

6 Discussion and conclusions

Our goal was to identify, characterize and visualize whether a given diffeomorphism has a blender or not. We showed that this can be achieved as follows.

- We identified the fixed points and computed their respective one-dimensional manifolds up to very large arclengths; these calculations are performed in a compactified phase space to account for large excursions of such manifolds;
- this manifold data was used to compute the hyperbolic set Λ and the tangent directions of its one-dimensional stable or unstable manifold, respectively, for different values of parameters

of interest; images of Λ and its one-dimensional invariant manifold in the compactified phase space are already rather suggestive of whether Λ has the carpet property or not;

- we verify the carpet property by considering the change in gap sizes between intersection points of an increasingly longer computed part of the one-dimensional invariant manifold of Λ with a suitable section; the convergence of the largest of these gaps with respect to the arclength of the manifold provides an effective numerical criterion.

These techniques were demonstrated for the three-dimensional Hénon-like family H , which is one of the very few explicit examples of a diffeomorphism with a blender. We identified the range of the shear parameter ξ (defining the center direction) where H has a blender and showed that infinitely many gaps emerge in the respective projection outside of this range. The study of bifurcations of blenders is an interesting topic and a subject of our ongoing research. To give a flavor, our investigation of intersection sets of one-dimensional manifolds indicates that we cannot at present exclude the possibility that, in between the gaps that form, there may be subregions or ‘stripes’ that are still filled up densely by the one-dimensional (un)stable manifold of Λ . This would mean that families of curve segments through these striped regions cannot avoid intersections, so that the carpet property may still be satisfied, albeit for a much smaller subset of the original blender. This would mean that the hyperbolic set Λ bifurcates from being a ‘large blender’ by breaking up into a much smaller sub-blender; this would be somewhat reminiscent of what is known as a basin boundary metamorphosis [11].

Blenders are robust phenomena and may, hence, be present in any given family of diffeomorphisms of dimension at least three. The issue is how to identify them if they exist. From the practical point of view, one needs to find in a given map a hyperbolic set and then check whether it is a blender. The work presented here should be seen as a feasibility study that demonstrates the availability of advanced numerical tools for this task. We have made use of the skew-product structure of the family H ; in particular, it allowed us to compute the hyperbolic set Λ by considering the intersection sets of one-dimensional invariant manifolds. When one is faced with other three-dimensional diffeomorphisms without this special structure, finding Λ will require one to find the intersection set between one-dimensional and two-dimensional invariant manifolds. Indeed, this is a more challenging task, but numerical methods for the computation of two-dimensional invariant manifolds do exist [17, 18]. However, one may be able to identify a fixed point or periodic point in Λ ; then it is entirely straightforward to compute its one-dimensional manifold and check for the carpet property. Hence, even though it is much more challenging to compute Λ itself, our numerical approach can verify whether it is blender or not. Therefore, from a practical point of view, it is perfectly feasible to apply the numerical techniques presented here also to more general three-dimensional diffeomorphisms. Of particular interest in this context will be Poincaré maps of four-dimensional vector fields. Indeed, such vector fields arise in numerous areas of application and there are many examples in the applied mathematics literature; promising candidates for a search for blenders in this context will be certain types of homoclinic and heteroclinic cycles [9, 13, 16] that give rise to recurrent dynamics in form of three-dimensional full horseshoes.

Blenders are closely associated with *robust heterodimensional cycles*, which are another important concept in the theory of non-uniformly hyperbolic systems [5]. A heterodimensional cycle of a diffeomorphism of dimension at least three consists of connecting orbits between two fixed or periodic points of different unstable indices. In dimension three, a blender Λ (of unstable index 2) can be used to construct heterodimensional cycles by providing robust intersections between

its one-dimensional stable manifold $W^s(\Lambda)$ and the one-dimensional unstable manifold of another hyperbolic set [3]. On the other hand, blenders can naturally emerge from a heterodimensional cycle via nearby saddle-node bifurcations that admit so-called strong homoclinic intersections [4]. Hence, the numerical techniques presented here may well be of relevance for the study of heterodimensional cycles.

In this context we mention that a heterodimensional cycle was identified, with numerical techniques based on two-point boundary-value problem formulations, in an explicit four-dimensional vector field model of intracellular calcium dynamics [25]. Recent work in [13] considers the intersection sets of the invariant manifolds of the respective periodic orbits with a three-dimensional Poincaré section; the heterodimensional cycle exists along a curve in the relevant parameter plane, and the study of the overall bifurcation diagram is ongoing work. It will be interesting but challenging to try to identify blenders in this system to see what roles they play.

Acknowledgments

The authors thank Andy Hammerlindl and Ale Jan Homburg for helpful discussions. We also thank the anonymous referees for their constructive comments, which helped us improve the presentation. The research of BK and HMO was supported by Royal Society Te Apārangi Marsden Fund grant #16-UOA-286, and that of KS by JSPS KAKENHI grant 18K03357.

References

- [1] A. Back, J. Guckenheimer, M. Myers, F. Wicklin and P. Worfolk, DsTool: Computer assisted exploration of dynamical systems, *Notices Amer. Math. Soc.*, **39** (1992), 303–309.
- [2] C. Bonatti, S. Crovisier, L. J. Díaz and A. Wilkinson, What is... a blender?, *Notices Amer. Math. Soc.*, **63** (2016), 1175–1178, URL <http://dx.doi.org/10.1090/noti1438>.
- [3] C. Bonatti and L. J. Díaz, Persistent nonhyperbolic transitive diffeomorphisms, *Ann. of Math. (2)*, **143** (1996), 357–396, URL <http://dx.doi.org/10.2307/2118647>.
- [4] C. Bonatti, L. J. Díaz and S. Kiriki, Stabilization of heterodimensional cycles, *Nonlinearity*, **25** (2012), 931–960, URL <http://dx.doi.org/10.1088/0951-7715/25/4/931>.
- [5] C. Bonatti, L. J. Díaz and M. Viana, *Dynamics beyond Uniform Hyperbolicity. A global geometric and probabilistic perspective*, vol. 102 of Encyclopaedia Math. Sci., Springer-Verlag, Berlin, 2005.
- [6] C. Bonatti and L. J. Díaz, Abundance of C^1 -robust homoclinic tangencies, *Trans. Amer. Math. Soc.*, **364** (2012), 5111–5148, URL <http://dx.doi.org/10.1090/S0002-9947-2012-05445-6>.
- [7] L. J. Díaz, S. Kiriki and K. Shinohara, Blenders in centre unstable Hénon-like families: with an application to heterodimensional bifurcations, *Nonlinearity*, **27** (2014), 353–378.
- [8] J. P. England, B. Krauskopf and H. M. Osinga, Computing one-dimensional stable manifolds and stable sets of planar maps without the inverse, *SIAM J. Appl. Dyn. Syst.*, **3** (2004), 161–190.

- [9] A. C. Fowler and C. T. Sparrow, Bifocal homoclinic orbits in four dimensions, *Nonlinearity*, **4**(4) (1991), 1159–1182.
- [10] R. Gilmore and M. Lefranc, *The Topology of Chaos: Alice in Stretch and Squeezeland*, Wiley-VCH, New York, 2002.
- [11] C. Grebogi, E. Ott and J. A. Yorke, Metamorphoses of Basin Boundaries in Nonlinear Dynamical Systems *Phys. Rev. Lett.*, **56** (1986), 1011.
- [12] J. Guckenheimer and P. Holmes, *Nonlinear Oscillations, Dynamical Systems and Bifurcations of Vector Fields*, Springer-Verlag, New York, 2nd edition, 1986.
- [13] A. Hammerlindl, B. Krauskopf, G. Mason and H. M. Osinga, Global manifold structure of a continuous-time heterodimensional cycle, arXiv 1906.11438, 2019.
- [14] M. Hénon, A two-dimensional mapping with a strange attractor, *Comm. Math. Phys.*, **50** (1976), 69–77.
- [15] S. Hittmeyer, B. Krauskopf, H. M. Osinga and K. Shinohara, Existence of blenders in a Hénon-like family: geometric insights from invariant manifold computations, *Nonlinearity*, **31** (2018), R239–R267.
- [16] A. J. Homburg and B. Sandstede, Homoclinic and heteroclinic bifurcations in vector fields, in H. Broer, F. Takens and B. Hasselblatt, *Handbook of Dynamical Systems*, vol. III Elsevier, Amsterdam, 2010, 379–524.
- [17] B. Krauskopf and H. M. Osinga, Growing 1D and quasi-2D unstable manifolds of maps, *J. Comput. Phys.*, **146** (1998), 404–419.
- [18] B. Krauskopf and H. M. Osinga, Globalizing two-dimensional unstable manifolds of maps, *Int. J. Bifurcation and Chaos*, **8**(3) (1998), 483–503.
- [19] B. Krauskopf and H. Osinga, Investigating torus bifurcations in the forced Van der Pol oscillator, in *Numerical Methods for Bifurcation Problems and Large-Scale Dynamical Systems (Minneapolis, MN, 1997)*, vol. 119 of IMA Vol. Math. Appl., Springer-Verlag, New York, 2000, 199–208.
- [20] J. Palis and W. de Melo, *Geometric Theory of Dynamical Systems*, Springer-Verlag, New York, 1982.
- [21] J. Palis and F. Takens, *Hyperbolicity and Sensitive Chaotic Dynamics at Homoclinic Bifurcations*, vol. 35 of Cambridge Stud. Adv. Math., Cambridge University Press, Cambridge, UK, 1993.
- [22] M. Shub, *Global Stability of Dynamical Systems* Springer-Verlag, New York, 1986.
- [23] M. Shub, What is ... a horseshoe?, *Notices Amer. Math. Soc.*, **52** (2005), 516–517.
- [24] S. Smale, Differentiable dynamical systems, *Bull. Amer. Math. Soc.* **73** (1967), 747–817.
- [25] W. Zhang, B. Krauskopf and V. Kirk, How to find a codimension-one heteroclinic cycle between two periodic orbits, *Discrete Contin. Dyn. Syst. Ser. A*, **32** (2012), 2825–2851.